Conclusion

A method is developed to find the initial stabilizing low-order output feedback dynamic compensator by using the LQG solution for an equivalent configuration and reducing the order. The compensator found by employing an approximate LTR technique offers a design with good performance.

References

[1]Syrmos, V. L., Abdallah, C., Dorato, P., and Grigoriadis, K., "Static Output Feedback—A Survey," *Automatica*, Vol. 33, No. 2, 1997, pp. 125–137.

[2]Levine, W. S., and Athans, M., "On the Determination of the Optimal Constant Output Feedback Gains for Linear Multivariable Systems," *IEEE Transactions on Automatic Control*, Vol. 15, No. 1, 1970, pp. 44–48.

[3]Moerder, D. D., and Calise, A. J., "Convergence of Numerical Algorithm for Calculating Optimal Output Feedback Gains," *IEEE Transactions on Automatic Control*, Vol. 30, No. 1, 1985, pp. 900–903.

[4]Calise, A. J., and Prasad, J. V. R., "Approximate Loop Transfer Recovery Method for Designing Fixed-Order Compensators," *Journal of Guidance, Control, and Dynamics*, Vol. 13, No. 2, 1990, pp. 297–302.

[5]Kucera, V., and DeSouza, C. E., "A Necessary and Sufficient Condition for Output Feedback Stabilizability," *Automatica*, Vol. 31, No. 9, 1995, pp. 1357–1359.

[6]Mukhopadhyay, V., Newsom, J. R., and Abel, I., "Reduced-Order Optimal Feedback Control Law Synthesis for Flutter Suppression," *Journal of Guidance, Control, and Dynamics*," Vol. 5, No. 4, 1982, pp. 50–54.

[7]Nichols, J. O., "Analysis and Compilation of Missile Aerodynamic Data, Volume 1, Data Presentation and Analysis," NASA CR-2835, May 1977.

[8]Sofonov, M. G., and Chiang, R. Y., "Robust Control Tool Box for Use with MATLAB," *User's Guide*, MathWorks, Natick, MA, 1986.

Dynamics of a Dual-Probe Tethered System

Joshua Ashenberg* and Enrico C. Lorenzini†
Harvard–Smithsonian Center for Astrophysics, Cambridge, Massachusetts 02138

I. Introduction

THE concept of a multiprobe tether has been recently proposed as a feasible configuration for a mission to collect data in the lower thermosphere.[1] Such a mission would be extremely valuable to atmospheric scientists who need to understand the cooling processes of the lower thermosphere, which are linked to global warming of the troposphere and ozone depletion in the stratosphere. The altitude of interest, 120–150 km, is not accessible to balloons or satellites. The atmosphere in this region is too rarefied for balloons and too dense for satellites. A long tether would allow probes to be lowered deep into the atmosphere from an orbiter positioned above. The multiprobe configuration offers the opportunity to measure the vertical gradient of the atmospheric properties under investigation. There are also other interesting applications for long tethers, such as wind-tunnel experiments under actual conditions and stereoscopic remote sensing of the Earth's surface.[2]

This Note treats the dynamics of a dual probe, where two probes, close to each other, are located at the far end of the tether. The system is designed to operate at the desired low altitudes and keep the tether oscillations bounded and small. The purpose of this research is to gain a preliminary understanding of the system dynamics suitable for a feasibility study and to select preliminary values of parameters for further investigation. The guideline of the research is to examine the influence of the various parameters on the system stability, assuming that the system starts from stable conditions (particularly, zero amplitude and zero rate). Small perturbations and modal analysis techniques are applied for analyzing the linear, i.e., small amplitude, motion. The nonlinear motion is analyzed by means of a systematic parametric study that uses numerical simulations and stroboscopic mapping techniques.

Received May 2, 1996; revision received April 18, 1997; accepted for publication June 20, 1997.

*Consultant, Radio and Geoastronomy Division, Mail Stop 80. Member AIAA.

†Staff Scientist, Radio and Geoastronomy Division, Mail Stop 80. Senior Member AIAA.

II. Model

The system under investigation consists of two small probes, m_1 and m_2, attached to a tether connected to a massive orbiter with mass M and orbital radius r. The tether length between the orbiter and the first probe is L_1, and the length between the probes is L_2. Typically $m_1 = 200\,\text{kg}, m_2 = 40\text{–}200\,\text{kg}$, and $M = 90{,}000\,\text{kg}$. Thus, the typical value of the probe mass ratio is $0.2 \le \epsilon_m \le 1$, where $\epsilon_m = m_2/m_1$. The second dimensionless parameter is the length ratio, defined as $\epsilon_L = L_2/L_1$. The length of the dual tether is about 100 km $(L_1 + L_2)$. Because L_2 typically is shorter than the local atmospheric scale height, i.e., 5 km, ϵ_L is a small parameter, i.e., $\epsilon_L \ll 1$. The orbiter moves in a small eccentricity orbit $(e < 0.01)$ around the Earth at an altitude of 220–250 km. Therefore, although the orbiter may be considered as drag-free for the duration of the mission, the atmospheric perturbations are significant when dealing with the dynamics of the probes. Generally speaking, the system dynamics is extremely complicated and requires tedious modeling and simulations. Because this research is primarily a parametric investigation, a reasonable model reduction must be applied to identify the characteristic dynamic behavior of the system. The main assumptions are that all satellites are in a single orbital plane, the satellites are point masses, and the tether is inelastic and massless. These are classic assumptions adopted by many authors working on tethered systems.[3]

The desired equations for the pitch tether angles α_1 and α_2 in terms of the true anomaly θ as the independent variable are derived from the Lagrangian function $L = K - V$. The kinetic energy K and the potential energy V are as follows:

$$\begin{aligned} K &= \tfrac{1}{2}MV_M^2 + \tfrac{1}{2}m_1\left(V_1^2 + \epsilon_m V_2^2\right) \\ &= \tfrac{1}{2}[M + (1+\epsilon_m)m_1](\dot r^2 + r^2\dot\theta^2) + \tfrac{1}{2}m_1\Big[L_1^2(1+\epsilon_m) \\ &\quad \times (\dot\alpha_1 + \dot\theta)^2 + 2L_1(1+\epsilon_m)(\dot\alpha_1 + \dot\theta)(\dot r\sin\alpha_1 - r\dot\theta\cos\alpha_1) \\ &\quad + \epsilon_m L_2^2(\dot\alpha_2 + \dot\theta)^2 + 2\epsilon_m L_2(\dot\alpha_2 + \dot\theta)(\dot r\sin\alpha_2 - r\dot\theta\cos\alpha_2) \\ &\quad + 2\epsilon_m L_1 L_2(\dot\alpha_1 + \dot\theta)(\dot\alpha_2 + \dot\theta)\cos(\alpha_1 + \alpha_2)\Big] \end{aligned} \tag{1}$$

and

$$\begin{aligned} V &= -\mu_\oplus\left[\frac{M}{r} + m_1\left(\frac{1}{r_1} + \frac{\epsilon_m}{r_2}\right)\right] \\ &= -\frac{\mu_\oplus M}{r} - \frac{\mu_\oplus(1+\epsilon_m)m_1}{r}\left[1 + \frac{L_1}{r}\cos\alpha_1\right. \\ &\quad \left. - \frac{1}{2}\frac{L_1^2}{r}\left(1 - 3\cos^2\alpha_1\right) + \frac{\epsilon_m}{1+\epsilon_m}\frac{L_2}{r}\cos\alpha_2 + O\left(\frac{L_1L_2}{r^2}\right)\right] \end{aligned} \tag{2}$$

where V_j represents the velocity of the j mass and $(\dot{})$ are time derivatives. Equation (2) is a result of a small-length ratio expansion, where terms of orders of magnitude $\{(L_1/r)^3 < L_1L_2/r^2\} \ll (L_1/r)^2$ are neglected. The equations of motion derived from the Lagrangian function are then expressed in terms of the true anomaly as follows:

$$\begin{aligned} &\left(1 + \epsilon_m\sin^2\Delta\alpha\right)(1 + e\cos\theta)\alpha_1'' - 2\left(1 + \epsilon_m\sin^2\Delta\alpha\right)e\sin\theta\alpha_1' \\ &\quad + \frac{1}{2}\epsilon_m(1 + e\cos\theta)(\alpha_1' + 1)^2\sin 2\Delta\alpha \\ &\quad + \epsilon_m\epsilon_L(1 + e\cos\theta)(\alpha_2' + 1)^2\sin\Delta\alpha \\ &\quad - 2\epsilon_m e\sin\theta\sin^2\Delta\alpha + \frac{3}{2}(1+\epsilon_m)\sin 2\alpha_1 \\ &\quad = 2e\sin\theta + \frac{r^3}{\mu_\oplus}\frac{1}{m_1L_1^2}\left(Q_{\alpha_1} - \frac{\cos\Delta\alpha}{\epsilon_L}Q_{\alpha_2}\right) \end{aligned} \tag{3}$$

$$\begin{aligned}
&\epsilon_L\left(1+\epsilon_m\sin^2\Delta\alpha\right)(1+e\cos\theta)\alpha_2'' \\
&\quad -2\epsilon_L\left(1+\epsilon_m\sin^2\Delta\alpha\right)e\sin\theta\alpha_2' \\
&\quad -(1+\epsilon_m)(1+e\cos\theta)(\alpha_1'+1)^2\sin\Delta\alpha \\
&\quad -\frac{1}{2}\epsilon_m\epsilon_L(1+e\cos\theta)(\alpha_2'+1)^2\sin 2\Delta\alpha \\
&\quad -2\epsilon_m\epsilon_L e\sin\theta\sin^2\Delta\alpha-\frac{3}{2}(1+\epsilon_m)\cos\Delta\alpha\sin 2\alpha_1 \\
&\quad =2\epsilon_L e\sin\theta-\frac{r^3}{\mu_\oplus}\frac{1}{m_1L_1^2}\left(\cos\Delta\alpha\,Q_{\alpha_1}-\frac{1+\epsilon_m}{\epsilon_m\epsilon_L}Q_{\alpha_2}\right) \qquad (4)
\end{aligned}$$

Here $\Delta\alpha=\alpha_1-\alpha_2$, α_1, and a_2 are the corresponding angles between the two parts of the tether and the local vertical, r is the orbital radius vector, $(\,)'$ are derivatives with respect to the true anomaly θ, and Q_j are the generalized forces.

III. Dynamic Analysis

A. Unperturbed Dynamics

Because motion with the smallest possible librations is desired, analysis of the linear oscillations is of great importance. The linear anomaly-dependent dynamics equations can be written in the form

$$\begin{aligned}
&(1+e\cos\theta)\alpha_1''-2e\sin\theta\alpha_1'+[3+\epsilon_m(4+e\cos\theta+\epsilon_L)]\alpha_1 \\
&\quad -\epsilon_m(1+\epsilon_L)(1+e\cos\theta)\alpha_2=2e\sin\theta \\
&\epsilon_L(1+e\cos\theta)\alpha_2''-2\epsilon_L e\sin\theta\alpha_2'-[(1+\epsilon_m)(4+e\cos\theta) \\
&\quad +\epsilon_m\epsilon_L]\alpha_1+(1+\epsilon_m+\epsilon_m\epsilon_L)(1+e\cos\theta)\alpha_2=2\epsilon_L e\sin\theta
\end{aligned} \qquad (5)$$

To reveal the zero-eccentricity dynamics and the first-order eccentricity excitation, the pitch angles are expanded for small eccentricities $\alpha_j=\alpha_j^{(0)}+e\alpha_j^{(1)}$; $j=1,2$. The resulting zero and first-order expansions are

$$e^0:\begin{cases}\alpha_1^{(0)\prime\prime}+(3+4\epsilon_m+\epsilon_m\epsilon_L)\alpha_1^{(0)}-\epsilon_m(1+\epsilon_L)\alpha_2^{(0)}=0\\ \epsilon_L\alpha_2^{(0)\prime\prime}-4(1+\epsilon_m)\alpha_1^{(0)}+(1+\epsilon_m+\epsilon_m\epsilon_L)\alpha^{(0)}=0\end{cases} \qquad (6)$$

and

$$e^1:\begin{cases}\alpha_1^{(1)\prime\prime}+(3+4\epsilon_m+\epsilon_m\epsilon_L)\alpha_1^{(1)}-\epsilon_m(1+\epsilon_L)\alpha_2^{(1)}\\ \quad=2\sin\theta+2\sin\theta\alpha_1^{(0)\prime}+3(1+\epsilon_m)\cos\theta\alpha_1^{(0)}\\ \epsilon_L\alpha_2^{(1)\prime\prime}-4(1+\epsilon_m)\alpha_1^{(1)}+(1+\epsilon_m+\epsilon_m\epsilon_L)\alpha_2^{(1)}\\ \quad=2\epsilon_L\sin\theta+2\epsilon_L\sin\theta\alpha_2^{(0)\prime}+3(1+\epsilon_m)\cos\theta\alpha_1^{(0)}\end{cases} \qquad (7)$$

The eigenvalues ω_j^2 and the eigenvectors $\boldsymbol{v}_j$ of the zero eccentricity system are

$$\omega_1\approx\sqrt{3}\left[1-\frac{5\epsilon_m}{2(1+\epsilon_m)}\epsilon_L\right]$$

$$\omega_2\approx\frac{\sqrt{1+\epsilon_m}}{\sqrt{\epsilon_L}}\left[1+\frac{5\epsilon_m}{2(1+\epsilon_m)}\epsilon_L\right] \qquad (8)$$

and

$$\boldsymbol{v}_1\approx\begin{pmatrix}1\\ 4+\dfrac{3(4-\epsilon_m)}{1+\epsilon_m}\epsilon_L\end{pmatrix}\qquad \boldsymbol{v}_2\approx\begin{pmatrix}1\\ -\dfrac{1+\epsilon_m}{\epsilon_m}\dfrac{1}{\epsilon_L}+\dfrac{4}{\epsilon_m}\end{pmatrix} \qquad (9)$$

Expressions (8) and (9) were expanded in small ϵ_L up to the first order of ϵ_L. The first eigenvalue indicates a frequency slightly lower than the single tether frequency ($\sqrt{3}$). This is because in our model the orbiter (rather than the system center of mass[4]) is constrained to follow a Keplerian orbit. This assumption reflects the real situation in which the orbiter is controlled to follow a given orbit and not the center of mass of the tethered system. The first eigenvector indicates that the amplitude ratio α_1/α_2 of this mode is about 1:4. Decreasing the mass ratio will increase the amplitude ratio. The second mode has a higher frequency that increases as the length ratio decreases. These results are compatible with numerical simulations of Eqs. (3) and (4).

The second-order system reveals the effect of the eccentricity excitation. Assuming null initial conditions and transforming the angles by means of $\boldsymbol{\alpha}=\boldsymbol{\Phi\eta}$, where $\boldsymbol{\Phi}$ is the modal matrix, the forced response is obtained as follows:

$$\eta_1=\frac{1+\epsilon_m+5\epsilon_m\epsilon_L}{\omega_1^2-1}\sin\theta\qquad \eta_2=\frac{3\epsilon_L+4\epsilon_L^2}{\omega_2^2-1}\sin\theta \qquad (10)$$

It is easy to see that the most likely resonance for η_1 exists for max ϵ_m and min ϵ_L, which satisfy the equation $2(1+\epsilon_m)-15\epsilon_m\epsilon_L=0$. The corresponding roots are $\epsilon_m=1$ and $\epsilon_L=0.26$. This contradicts the assumption of small ϵ_L, which is being considered in this analysis. For η_2, the condition is min ϵ_m and min ϵ_L, which implies $1+\epsilon_m+(5\epsilon_m-1)\epsilon_L=0$. There are no feasible parameters that satisfy this condition. Because the resonance curves always start at zero eccentricity, these results exclude any possibility of eccentricity resonance for the configuration under investigation.

It is logical to seek a solution for the motion of the first probe as an asymptotic expansion in small ϵ_L. The procedure consists of expanding the angles as $\alpha_j=\alpha_j^{(0)}+\epsilon_L\alpha_j^{(1)}$, substituting them into the equation of motion, thus forming the zero (ϵ_L^0) and the first-order (ϵ_L^1) expansions. The major results are the following: the zero-order expression reveals the amplitude ratio, which is approximately 4:1,

$$\alpha_2^{(0)}=\frac{4+e\cos\theta}{1+e\cos\theta}\alpha_1^{(0)} \qquad (11)$$

and $\alpha_1^{(0)}$ satisfies the equation of motion for a single tether, as expected. The equations have been solved by applying the WKBJ method.[5,6] After carrying out the procedure, the zero-order particular solutions are

$$\begin{aligned}
\alpha_1^{(0)}&=\frac{e}{1+e\cos\theta}\left(\sin\theta-\frac{1}{\sqrt{3}}\sin\sqrt{3}\,\theta\right)\\
\alpha_2^{(0)}&=e\frac{4+e\cos\theta}{(1+e\cos\theta)^2}\left(\sin\theta-\frac{1}{\sqrt{3}}\sin\sqrt{3}\,\theta\right)
\end{aligned} \qquad (12)$$

The next order reveals a nonuniformity in the expansion because of the presence of the $\sqrt{3}$ frequency in the forcing term. To eliminate the resulting secular term, a renormalization[7] process is carried out. We modified the frequency $\omega=\sqrt{3}+\epsilon_L\omega_1$ and found that $\omega_1\approx-[2\epsilon_m(4+\epsilon_m)/\sqrt{3}(1+\epsilon_m)]$ eliminates the secular term. The resulting particular solutions are as follows:

$$\begin{aligned}
\alpha_1&=\frac{e}{1+e\cos\theta}\left\{\sin\theta-\frac{1}{\sqrt{3}}\sin\omega\theta\right.\\
&\quad\left.+\frac{\epsilon_L}{1+\epsilon_m}\left[(5+2\epsilon_m)\sin\theta-\frac{1}{3\sqrt{3}}(23+8\epsilon_m)\sin\omega\theta\right]\right\}\\
\alpha_2&=\frac{e}{(1+e\cos\theta)^2}\left((4+e\cos\theta)\left(\sin\theta-\frac{1}{\sqrt{3}}\sin\omega\theta\right)\right.\\
&\quad+\epsilon_L\frac{6}{1+\epsilon_m}\left\{\left[1+\frac{2}{3}\epsilon_m(5+2\epsilon_m)\right]\sin\theta\right.\\
&\quad\left.\left.-\frac{2}{\sqrt{3}}\left[1+\frac{1}{9}\epsilon_m(23+8\epsilon_m)\sin\omega\theta\right]\right\}\right)
\end{aligned} \qquad (13)$$

where

$$\omega=\sqrt{3}\left[1-\frac{2\epsilon_m(4+\epsilon_m)}{3(1+\epsilon_m)}\epsilon_L\right]$$

B. Atmospheric-Drag Perturbed Dynamics

For a typical atmospheric mission, the influence of the atmospheric drag on the tether and the probes must be taken into account, whereas the effect on the orbiter can be neglected because of the difference of a few scale heights between the orbiter and the probes. Moreover, to make the analysis manageable, we assume a spherical atmosphere with exponential density variation and constant scale height. The generalized forces due to drag are derived from the principle of virtual work, i.e., $\delta W = Q_r \delta r + Q_\theta \delta\theta + Q_{\alpha_1}\delta\alpha_1 + Q_{\alpha_2}\delta\alpha_2$, where

$$\delta W = \int_{s=0}^{L_1+L_2} \boldsymbol{f}(s) \cdot \delta \boldsymbol{r}(s)\, \mathrm{d}s$$

An interesting result, skipping the mathematical manipulations, is that the steady-state pitch α_j^s ratio in a circular orbit for small angles satisfies the following approximation:

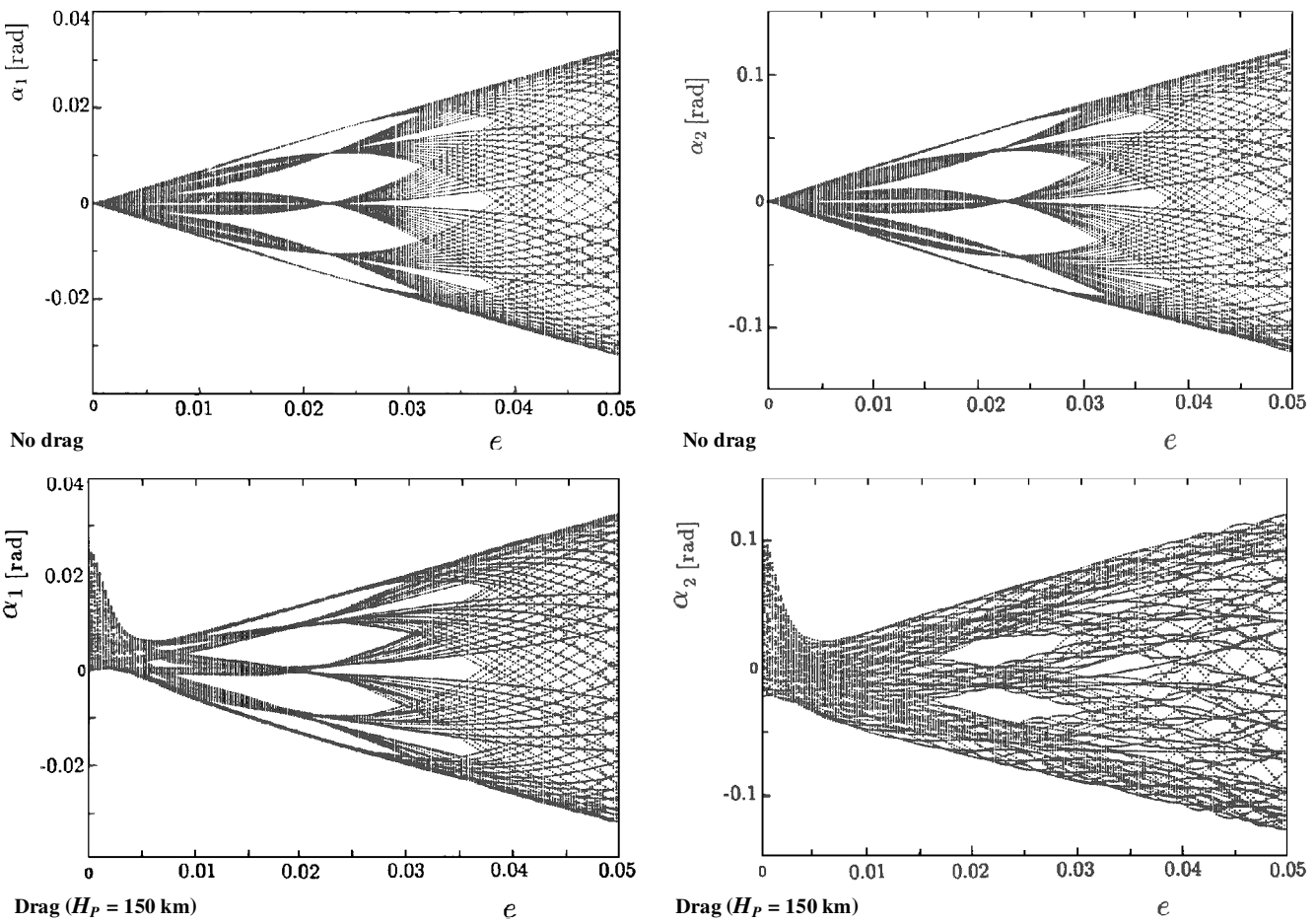

Fig. 1 Pitch angle and bifurcation.

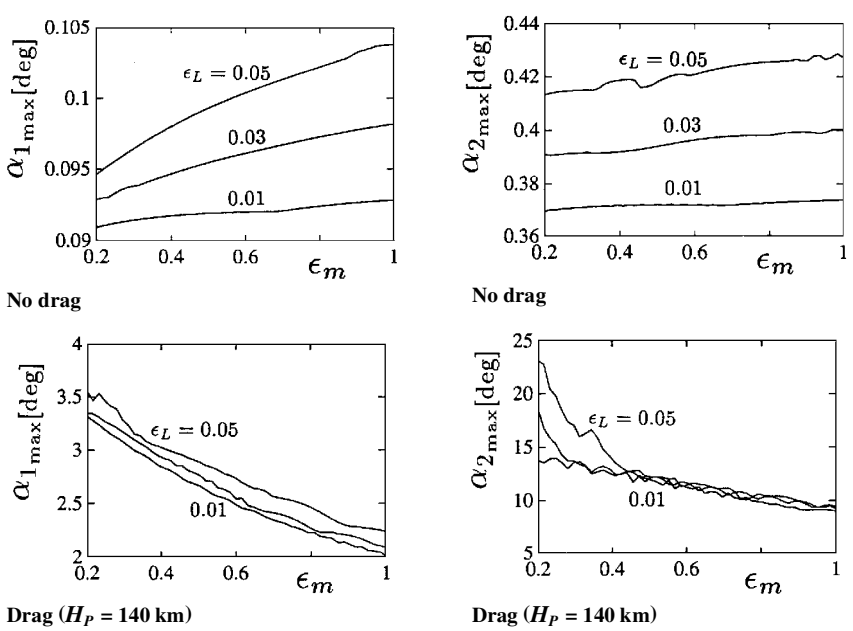

Fig. 2 Pitch amplitude vs mass ratio and length ratio.

$$\frac{\alpha_2^s}{\alpha_1^s} = 1 + \frac{3(1+\epsilon_m)}{\epsilon_m} \times \frac{\left(C_{D_t}/C_{D_P}\right)(dH/A_1)\left[1-(H/L_2)+(H/L_2)e^{-L_2/H}\right]+\epsilon_m^{\frac{2}{3}}}{\left(C_{D_t}/C_{D_P}\right)(dH/A_1)+e^{-L_2/H}+\epsilon_m^{\frac{2}{3}}} \tag{14}$$

where H is the scale height, C_{D_t} and C_{D_P} are the drag coefficients for the tether and the probes, respectively, d is the tether diameter, and A_1 and A_2 are the probe frontal areas. These can be related to the mass ratio by assuming mass-volume similarity, i.e., $A_2/A_1 = \epsilon_m^{2/3}$. This relationship indicates that the most influential parameters are H/L_2 and ϵ_m. Decreasing these quantities increases the pitch angle ratio. Generally, the dynamic response is due to the combined influence of the drag and the eccentricity. The drag-perturbed differential equations were linearized and solved by the WKBJ method. The conclusion is that, although the drag alters the dynamics by adding new even-periodic terms, a small drag causes a bounded motion with no resonance.

The influence of the drag can be observed by plotting the bifurcation of the angles with the eccentricity as the bifurcation parameter (Fig. 1). These plots are a stroboscopic sampling of the phase plane at each perigee passage. The initial conditions are zero so that the plots describe the eccentricity excitation for a variety of eccentricities. The atmospheric drag breaks the pitch symmetry (which can be inferred from the structure of the differential equations) and alters the periodic solution. A possible explanation for the amplification of the drag effect at low eccentricity is its noncommensurability with the eccentricity excitation. Also, because the perigee altitude is kept constant, the average drag varies as $(1-e)$ and, consequently, a circular orbit has the highest drag effect. A penetration down to altitudes less than $H_p = 130$ km without any tether control system appears feasible for a single-probe tethered system, whereas the stability of the lowest probe in a dual-probe system is more marginal. Figure 2 shows the roles of ϵ_m and ϵ_L within the attitude dynamics of the system with and without drag. Increasing ϵ_L increases the amplitudes of the pitch motion, whereas ϵ_m plays the opposite role in the perturbed and unperturbed dynamics.

IV. Concluding Remarks

The dual-probe configuration examined in this Note seems suitable for reaching altitudes as low as 130 km in the Earth's atmosphere. A single-probe tether system is preferable for reaching even lower altitudes. The dynamic behavior of the dual-probe system is characterized by a typical amplitude ratio of 4:1 between the pitch angles of the lower and upper probes. This ratio becomes larger at low altitudes when the upper tether performs small librations and the lower probe oscillates more strongly. The eccentricity excitation results in bounded oscillations for small eccentricities. A small length ratio is preferable, especially at low altitudes, because the drag acting on the lower tether induces large pitch oscillations on the lowest probe. The analytical results are comparable with numerical simulations of the equations of motion. The release of some simplifying assumptions by including, for example, tether flexibility and elasticity, has small effects for small librations and tethers of suitable stiffness.[2]

References

[1]Lorenzini, E. C., Cosmo, M. L., Grossi, M. D., Chance, K., and Davis, J. C., "Tethered Multi-Probe for Thermospheric Research," *Proceedings of the Fourth International Conference on Tethers in Space* (Washington, DC), Science and Technology Corp., Hampton, VA, 1995, pp. 1567–1576.

[2]Beletsky, V. V., and Levin, E. M., *Dynamics of Space Tether System, Advances in the Astronautical Sciences*, Vol. 83, American Astronautical Society, San Diego, CA, 1993, pp. 20–33.

[3]Misra, A. K., and Modi, V. J., "A Survey of the Dynamics and Control of Tethered Satellite Systems," *Advances in the Astronautical Sciences, Tethers in Space*, Vol. 62, 1986, pp. 667–719.

[4]Misra, A. K., Amier, Z., and Modi, V. J., "Attitude Dynamics of Three-Body Tethered System," *Acta Astronautica*, Vol. 17, No. 10, 1988, pp. 1059–1068.

[5]Cunningham, W. J., *Introduction to Nonlinear Analysis*, McGraw–Hill, New York, 1958, pp. 253–257.

[6]Modi, V. J., and Brereton, R. C., "Libration Analysis of a Dumbbell Satellite Using the WKBJ Method," *Journal of Applied Mechanics*, Vol. 33, No. 3, 1966, pp. 676–678.

[7]Nayfeh, A. H., and Mook, D. T., *Nonlinear Oscillations*, Wiley-Interscience, New York, 1979, p. 556.

Dynamical Characteristics of a Tethered Stabilized Satellite

Joshua Ashenberg* and Enrico C. Lorenzini†
Harvard–Smithsonian Center for Astrophysics, Cambridge, Massachusetts 02138

Nomenclature

A	= tether cross-section area
E	= tether material Young's modulus
f	= orbit true anomaly
L	= tether length
M	= satellite mass
m	= ballast mass
$\boldsymbol{r}$	= satellite orbit radius vector
T	= tether tension
$\alpha_1, \alpha_2, \alpha_3$	= satellite roll, pitch, and yaw angles
δ_1, δ_2	= roll and pitch control angles
θ_1, θ_2	= tether roll and pitch angles
μ	= gravitational constant
ρ	= offset of attachment point with respect to satellite center of mass
ρ_m	= tether material density
Ω	= orbital angular velocity
ω	= satellite angular velocity

I. Introduction

THE restoring torque of a gravity gradient-stabilized satellite can be enhanced significantly by adding a tether.[1] A possible way to stabilize an Earth-pointing satellite is by attaching the tether, with a ballast at its opposite end, to the leeward side of the satellite. A further improvement can be obtained by moving the attachment point over a two-dimensional surface.[2] This modification changes the stabilization method from passive to active. This concept may be very attractive for satellites with moderate-to-high pointing accuracy requirements that could be achieved by means of a low-energy controller.

This work presents a preliminary investigation of the stability characteristics of a tethered satellite attitude with respect to the local vertical. Other relevant topics analyzed are the influence of orbital eccentricity and tether oscillations on the satellite dynamics and identification of possible resonances. Parameters that affect the attitude control are the tether length, the offset between the satellite center of mass and the attachment point, and the ballast mass. The configuration under investigation consists of a satellite, a tether, and a ballast mass at the opposite end of the tether. The position of the movable tether attachment point is controlled by the stabilization control logic. To separate the tether dynamics from the satellite dynamics, we assume realistically that $\rho \ll L$ (typically $\rho < 1m$

Received Aug. 8, 1996; revision received April 23, 1997; accepted for publication June 23, 1997.

*Consultant, Radio and Geoastronomy Division, Mail Stop 80. Member AIAA.

†Staff Scientist, Radio and Geoastronomy Division, Mail Stop 80. Senior Member AIAA.